Preprint Title	Design and Characterization of Stable β-Caryophyllene-loaded Nanoemulsions: A Rational HLB-Based Approach for Enhanced Volatility Control and Sustained Release
Authors	Eduarda R. Baranda, Júlia S. Santos, Anna L. M. M. Toledo and Thaís N. Barradas
Publication Date	30 Mai 2025
Article Type	Full Research Paper
ORCID® iDs	Júlia S. Santos - https://orcid.org/0000-0002-7441-1940; Thaís N. Barradas - https://orcid.org/0000-0002-6558-9595

Design and Characterization of Stable β-Caryophyllene-loaded Nanoemulsions: A Rational HLB-Based Approach for Enhanced Volatility Control and Sustained Release

Eduarda Rios Baranda [1], Júlia Scherer Santos [2,3], Anna Lecticia M. Martinez Toledo [4], Thais Nogueira Barradas [3,5*]

[1] Postgraduate program in Pharmaceutical Sciences, Federal University of São Paulo, São Paulo, Brazil,

[2] Department of Pharmacology, Federal University of Juiz de Fora, Juiz de Fora, Brazil,

[3] Núcleo de Desenvolvimento e Tecnologia Farmacêutica, Federal University of Juiz de Fora, Brazil

[4] Instituto de Macromoléculas Professora Eloisa Mano, Federal University of Rio de Janeiro, Brazil.

[4] Instituto de Macromoléculas Professora Eloisa Mano, Federal University of Rio de Janeiro, Brazil.

Email: Thais Nogueira Barradas - thaisbarradas@ima.ufrj.br

* Corresponding author

Abstract

Phytochemicals with therapeutic potential have garnered increasing interest in recent years for their natural origin, multi-target pharmacological effects, and generally favorable safety profiles. One such compound, β-caryophyllene (BCP), a bicyclic sesquiterpene found in essential oils of various plants such as Cannabis sativa, Clove (*Syzygium aromaticum*), and Black pepper *(Piper nigrum*), has demonstrated promising analgesic, anti-inflammatory, antioxidant, and anticancer properties. Its activity as a selective CB2 receptor agonist has made BCP an especially attractive candidate for developing novel anti-inflammatory and neuroprotective therapies. BCP faces significant challenges in pharmaceutical formulation due to its volatility, low stability under acid environments, and low aqueous solubility. To address these limitations, we developed and characterized BCP-loaded nanoemulsions as a nanocarrier system to improve stability and bioavailability. A systematic, quantitative approach was employed to determine the optimal hydrophilic-lipophilic balance (HLB) for surfactants used in formulation, yielding an optimal range between 12.0 and 14.5. Ternary phase diagrams revealed that nanoemulsions could be obtained under high water content (>70%), low oil content (<10%), and minimal surfactant concentration. Nevertheless, colloidal stability experiments indicated that a co-surfactant was needed to avoid coalescence. In this context, nanoemulsions incorporating 6–8% BCP showed high encapsulation efficiency (>90%) and exhibited kinetic stability for up to 90 days, as confirmed by thermogravimetric analysis (TGA) and visual inspection. Notably, BCP evaporation was significantly reduced in optimized formulations. These findings highlight the critical role of tailored surfactant selection in nanoemulsion stability and offer valuable insights into the design of stable, scalable nanoformulations for hydrophobic phytochemicals.

Keywords: phytocannabinoid; nanoemulsions, pharmaceutical development, nanotechnology, sesquiterpenes

1. Introduction

The effort for sustainable nature-friendly resources of novel bioactive compounds has led to the search of new sources of phytochemical compounds as new potential therapeutic drugs. Beta-caryophyllene (BCP), a bicyclic sesquiterpene phytocannabinoid compound found in Oregano (*Origanum vulgare L*.) [1], Black Pepper (*Piper nigrum* L.) [2] , and Cinnamon (*Cinnamomum* spp.) [3], as well as in the oleoresin of *Copaiba* species (*Copaifera* L.) [4] shows promising use as anti-inflammatory shows promising use as anti-inflammatory [1,2], anti-bacterial [5], skin repair [6,7] as well as in the treatment of neurological and cognitive disorders [8,9]. Its activity as a selective CB2 receptor agonist has made BCP an especially attractive candidate for developing novel anti-inflammatory and neuroprotective therapies [1,8]. To overcome these issues, advanced drug delivery systems, particularly nanotechnology-based approaches, have been developed and show promising results.

Despite the pharmacological potential in both clinical and preclinical experiments, the formulation of BCP into stable and bioavailable dosage forms is challenging due to its volatility, hydrophobicity, acid sensitivity, and susceptibility to oxidation, which limit its clinical translation [3]. Conventional formulations fail to ensure sustained delivery and protection from environmental degradation, severely limiting BCP's clinical translation [10,11].

Despite the pharmacological potential in both clinical and preclinical experiments, the formulation of BCP into stable and bioavailable dosage forms is challenging due to its volatility, hydrophobicity, acid sensitivity, and susceptibility to

oxidation, which limits its clinical translation. Conventional formulations fail to ensure sustained delivery and protection from environmental degradation, severely limiting BCP's clinical translation. In this context, nanostructured lipid carriers, solid lipid nanoparticles [12], nanocapsules [13], self-emulsifying drug delivery systems [14] and cyclodextrin-based inclusion complexes [11] constitute effective strategies to enhance BCP's solubility and oral bioavailability, protecting it from environmental degradation, oxidation, and acid sensitivity [10]. Moreover, they provide sustained and controlled release, enabling targeted delivery either for topical or intranasal routes. Therefore, nanotechnology-enabled approaches improve pharmacological efficacy and increase clinical translation potential of novel bioactive molecules. Not only do these drug delivery systems address the major formulation challenges of BCP, they also pave the way for its broader pharmaceutical and therapeutic application.

Nanoemulsions (NE), are versatile and scalable nanocarrier systems for lipophilic and volatile drugs. NE are kinetically stable, oil-in-water colloidal dispersions with droplet sizes typically ranging from 20 to 200 nm [15]. They enhance bioavailability, solubility, stability, and permeability, while also allowing controlled release and targeted delivery [16]. However, the design and optimization of nanoemulsions require careful tuning of interfacial properties, which are influenced by surfactant type, concentration, temperature, oil phase composition, and the hydrophilic-lipophilic balance (HLB) [17]. Previous reports showed that HLB value of non-ionic surfactants significantly affected the droplet size and stability of nanoemulsions, with an optimal HLB value resulting in smaller droplet sizes and enhanced stability [18,19]. By optimizing these parameters, researchers can develop nanoemulsions with droplet sizes ranging from 20 to 200 nm, offering improved drug solubilization capacity and potential for enhanced therapeutic efficacy [17].

Although numerous studies have explored NEs as a carrier for essential oils and terpenes, including BCP [16], a few ones have performed a quantitative and systematic approach to determine the optimal HLB for BCP-based NEs [20,21]. Furthermore, long-term stability data, particularly under variable loading concentrations and storage conditions, remain scarce.

In this work, we report on the formulation, characterization, and stability analysis of BCP-loaded nanoemulsions, guided by a rational determination of the required HLB range for optimal formulation. Using ternary phase diagrams, we identified favorable oil:surfactant:water mixture zones and assessed how BCP loading affected encapsulation efficiency, volatility, drug release and kinetic stability. Thermogravimetric analysis (TGA) was employed to assess evaporation rate, offering insights into the protective role of the NE template for volatile compounds. Our results provide valuable preliminary data for the formulation of stable, effective nanoemulsions for lipophilic phytotherapeutics and support the translation of BCP into functional nanomedicine.

2. Material and Methods

2.1 Materials

β-Caryophyllene (BCP), along with all polymers and solvents used in this study, were purchased from Sigma-Aldrich Chemical Company (St. Louis, USA). Other reagents were obtained as follows: poloxamer 188 (Kolliphor P188 Micro, BASF, USA), ultrapure Milli-Q water (Millipore, USA), HPLC-grade methanol and acetonitrile (Synth, São Paulo, Brazil), phosphate-buffered saline (PBS, Gibco, Karlsruhe, Germany), and PEG-40 hydrogenated castor oil and Sorbitan monooleate (Neon, São Paulo, Brazil, Cellulose acetate filter membranes with 0.1-µm pore size, 75% porosity and 150-µm thickness (model VCWP04700, Millipore®, Darmstadt, Germany).

2.2. HLB determination

The hydrophilic-lipophilic balance (HLB) required for the stabilization of BCP emulsions was determined using emulsifier blends based on their individual HLB values [22–24]. 5 g of each emulsion were prepared in triplicate, containing 85% (w/w) of distilled water, 5% (w/w) of BCP and 10% (w/w) of a mixture of surfactants.

Analysis of creaming and phase separation after one day of manipulation supported the identification of the most stable formulation required for HLB determination. PEG-40 hydrogenated castor oil (HLB = 16) served as the most hydrophilic surfactant, and sorbitan monooleate (HLB = 4.3) as the most lipophilic surfactant. The aqueous phase (PEG-40 hydrogenated castor oil + water) was added to the oil phase (BCP + sorbitan monooleate) under magnetic stirring, followed by homogenization using an Ultra-Turrax (IKA T10 basic) for 30 seconds. HLB values ranging from ~8 to 16 were prepared by blending the emulsifiers and the BCP, as indicated in Table 1. Initial screening using five emulsions (E1–E5) were produced with HLB from ~8 to 16. Then, a refined batch of four additional emulsions (E6–E9) were prepared within the HLB range from ~13 to ~14, as shown in Table 1 and processed under ultrasonication at 90% of amplitude for 5 min under ice bath. To determine the required HLB (rHLB) of BCP, stability parameters were evaluated for E6 to E9, including creaming and phase separation occurrence, droplet size, and polydispersity (PdI) [11],[25], which were measured by Dynamic Light Scattering (DLS).

2.3 Ternary Phase Diagram

Emulsions determined to have appropriate HLB values and visual stability were selected for ternary phase diagram analysis using the aqueous titration method, as previously described [26]. Nine precursor mixtures with surfactant-to-oil ratios of 1:9, 2:8, 3:7, 4:6, 5:5, 6:4, 7:3, 8:2, and 9:1 were prepared to identify optimal formulation regions.

2.4 NE production and Droplet size measurements

Formulations falling within the NE region of the phase diagram were produced using an ultrasonic processor (Ultrasonics, USA) operating at 90 W in an ice bath for 5 minutes. Particle size and polydispersity index (PdI) were measured using dynamic light scattering (Zetasizer Nano ZS, Malvern Instruments). Stability assessments were performed at room temperature over 90 days, with mean droplet size and PdI measurements taken after preparation and on days 14, 21, 28, 60, and 90. Results represent the mean of three independent batches.

2.5 pH Measurements

A calibrated pHmeter was used to measure the initial pH of the freshly prepared NEs and stored samples at controlled room temperature in sealed containers. The records of pH values were taken at various time intervals (0, 1, 7, 14, 30, 60, and 90 days) to assess stability over time. Measurements were taken from at least three independent batches.

2.6 Isothermal TGA for Volatility Control

BCP-loaded NEs and a control sample composed of neat BCP were analyzed in a TGA Discovery 55 thermogravimetric analyzer calibrated for ambient drift. Set it to an isothermal mode at a temperature that mimics storage conditions or slightly elevated conditions (e.g., 50–60 °C) to accelerate the volatility process without causing decomposition.

Samples were submitted to a temperature ramp (10 °C/min) to 55°C and maintained under this temperature. The measurements occurred continuously recording the weight of the sample for 4 hours. At least three replicates per sample were conducted to ensure reproducibility. A plot of weight loss (%) vs. time was plotted

and the results were fitted to kinetic models if applicable (zero-order or first-order loss kinetics).

2.7 Encapsulation efficiency (EE%) and Drug loading (%)

Encapsulation efficiency (EE%) of BCP-loaded nanoemulsions was performed by calculating the percentage difference between the total concentration of BCP in nanoemulsion and the BCP concentration in the supernatant [27] . For determination of the BCP encapsulation, a calibration curve was obtained from stock solutions containing 0.4 µL/m of BCP into methanol by spectrophotometry at 205 nm (Varian Cary 50 UV-VIS Spectrophotometer). Nanoemulsions were centrifuged at 4000 RPM for 30 minutes and the supernatant was submitted to spectrophotometer analysis at 205 nm [28].

EE (%) in NEs was determined as the percentage difference between the total concentration in the NEs and the concentration found in the supernatant (Equation 1). The results are expressed as the average of three measurements.

2.8 *In vitro* BCP release using Franz Cell Apparatus

The BCP-loaded NEs and a control sample composed of neat BCP (1 ml of each) were applied to the donor compartment of the Franz cell onto a suitable synthetic membrane (0.1 µm pore size, 75% porosity, 150 µm thickness; Millipore®, Germany). A physiologically relevant release medium was chosen to simulate in vivo conditions and ensure sink conditions for BCP. Release Medium was composed by phosphate-buffered saline (PBS, pH 7.4) supplemented with 1% Tween 80 [29].

The receptor compartment was filled with 15ml of the release medium maintained at 37 °C, with continuous stirring. At predetermined time points (0, 0.5, 1, 2, 4, 6 and 8 hours), withdraw samples from the release medium. The withdrawn

volume was replaced with fresh medium to maintain sink conditions. The amount of BCP released was quantified using HPLC using Agilent 1260 Infinity II, a C18 reverse-phase column (250 mm × 4.6 mm, 5 µm) (FR-Thermo Scientific, 250 × 4.6 mm, 5 µm, 25 °C) [13].

A UV-VIS detector was used at 210 nm. Mobile Phase was composed by acetonitrile, methanol, and water (8:1:1, v/v/v), at 1.0 mL/min, injection volume of 20 µL Retention Time of ~5.5 min for BCP confirmed the reproducibility of the method reported in literature[13]. The method was partially validated according to ICH Q2(R1) guidelines for linearity (R2 = 0.9998), accuracy (recovery ~98–102%), and precision (RSD < 2%) [30].

Tests were performed in triplicate to ensure statistical validity. The data was expressed as cumulative percentage release vs. time. The released data were fitted to kinetic models (e.g., zero-order, first-order, Higuchi, or Korsmeyer–Peppas models) to determine the release mechanism using DDSolver Excel Add-in [31].

2.9 Data Analysis

Measures were performed in triplicate. Data statistical analysis was performed by one-way analysis of variance (ANOVA) with Tukey post-test in OriginLab 9.0. Regression analysis was performed in OriginLab 9.0.

3. Results and Discussion

3.1 HLB Optimization and Emulsion Screening

Initial screening using five emulsions (E1–E5) revealed that formulations E3 and E4 yielded optimal physical stability with no creaming of phase separation observation within 24h. As shown in Table 1, these corresponded to a HLB range between 12.958 and 14.362, supporting the hypothesis that BCP requires a moderately hydrophilic

surfactant system. Such HLB range ensured improved solubility and dispersion of BCP, as moderately hydrophilic surfactant blend could effectively reduce interfacial tension between the hydrophobic BCP oil phase and the aqueous phase, providing stable oil-in-water macroemulsions [32].

To refine this range, four additional emulsions (E6–E9) were prepared within this rHLB window and processed to obtain NE. The optimal NE characteristics, including the smallest particle size and lowest PdI, were found in E9, with rHLB of ~14,4 (Figure 1). Optimal HLB values have been reported to minimize droplet size of NE prepared with surfactant mixtures. HLB values close to the rHLB of the oil phase can produce the smallest droplet sizes and narrowest size distributions. For example, in lemon myrtle NEs, the smallest droplet sizes (~66 nm) and lowest PdI were observed at HLB 13–14 [33].

Although numerous studies have developed NE for essential oils containing BCP, few have applied a quantitative and systematic approach to determine the optimal HLB specifically for BCP-based NE. Previous reports showed the rHLB value for copaiba oil, mainly composed by BCP was found to be 15.0, and was responsible for producing the most stable NE, characterized by the smallest droplet size, low PdI, with no phase separation. This value closely matched the rHLB of BCP found here, highlighting the importance of matching surfactant HLB to the oil phase to achieve optimal stability and droplet size in BCP-loaded NE [20,21].

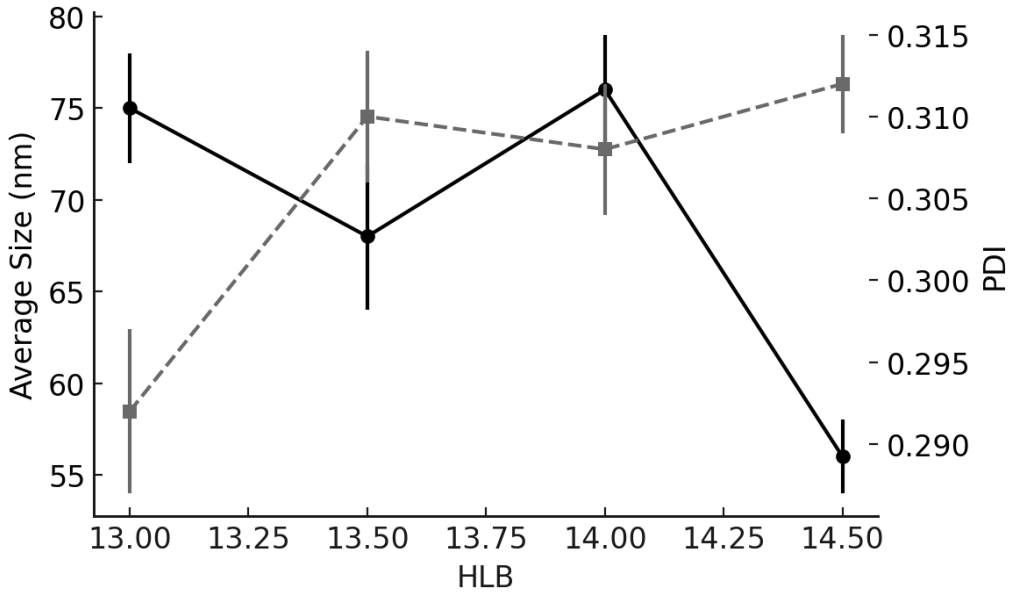

Figure 1: Effect of HLB on Average Particle Size and Polydispersity Index (PdI) in BCP NE. Average particle size (black solid line) and PdI (gray dashed line) are plotted as a function of the hydrophilic-lipophilic balance (HLB) of the surfactant mixture. The smallest droplet size (51.7 ± 2.1 nm) was observed at HLB 14.362. All formulations showed low PdI values (≤ 0.312), indicating monodisperse and stable emulsions. Error bars represent ± standard deviation from three independent replicates**.**

Regarding long-term stability, NE with the optimized rHLB (15.0) maintained their physical stability, appearance, and droplet size distribution over at least two months under ambient storage conditions [21]. However, comprehensive data on stability under varying loading concentrations of neat BCP remain scarce in the literature.

Other reports on essential oil nanoemulsions emphasize that systematic optimization techniques such as response surface methodology (RSM) can be used to fine-tune formulation variables including oil concentration, surfactant type and ratio

(thus HLB), and stirring speed to maximize stability and performance [34] . Yet, these approaches have been less frequently applied specifically to BCP nanoemulsions, leaving a gap for more rigorous, quantitative optimization studies.

As observed in Figure 1, droplet size varied non-linearly with HLB. As the HLB value increases from low to optimal, droplet size decreases, but beyond the optimal HLB, droplet size tends to increase again. This pattern reflects changes in the interfacial layer structure and surfactant packing around droplets [19,32]. The HLB reflects how surfactant molecules can effectively reduce interfacial tension and stabilize the oil droplets. Surfactants with HLB values matching the oil's rHLB form a compact, stable interfacial film, preventing coalescence and leading to smaller, more uniform droplets [35].

Additionally, the HLB influences the PdI of NE by affecting the uniformity and size distribution of the droplets. It is known that lower PdI values reflect more uniform droplet sizes and are generally achieved at optimal HLB values that closely match the rHLB of the oil phase. For instance, lemon myrtle NE showed the lowest PdI (~0.23) at HLB 13–14 with Tween 80-Span 80 mixtures, indicating a narrow droplet size distribution and higher uniformity [33]. As depicted in Figure 1, increasing HLB values can lead to a decrease in PdI up to an optimal point, after which PdI may increase again [36]. This trend reflects improved interfacial stabilization near the optimal HLB, resulting in more homogeneous droplets, while deviation from this balance causes fewer stable interfaces and broader size distributions.

It is noteworthy that while HLB strongly affects droplet size, its impact on PdI can be less pronounced depending on formulation specifics. In this context, soybean oil-loaded NE showed PdI values in a narrow range (0.071–0.117) across different HLB values, with no significant changes in PdI despite significant variations in droplet

size [18], meaning that the exact influence of HLB on PdI remain to be investigated.

3.2 Ternary Phase Diagram Behavior

Ternary phase diagrams reveal distinct formulation regions, including macroemulsions, nanoemulsions, gels, and phase separation (Figure 2). NE can be formed when the surfactant concentration is sufficient to stabilize the small oil droplets; phase separation occurs at higher oil and lower surfactant concentrations due to insufficient interfacial coverage. Gel was obtained when higher oil (up to 60%) and surfactants concentrations (between 20-70%) were combined. Gel regions identified with surfactant content ≥30% and oil ≥60%, which is consistent with gelation previously reported for castor oil-based polyoxyethylene surfactants [37].

High surfactant concentrations combined with large oil phases can lead to structured, viscous gel networks rather than fluid emulsions. This gelation occurs through various mechanisms involving surfactant self-assembly. In water/nonionic surfactant/oil systems, gel-emulsions form through a process of multiple emulsification, resulting in high-internal-phase-volume W/O emulsions with submicrometer water droplets [38]. Liquid crystal formation by surfactants plays a crucial role in stabilizing intermediate multiple emulsions during the inversion process, leading to stable gel emulsions [39]. The presence of lamellar liquid crystalline phases during emulsification can result in finer, more homogeneous emulsions due to their favorable properties, including high oil solubilization capacity and low interfacial tension [40].

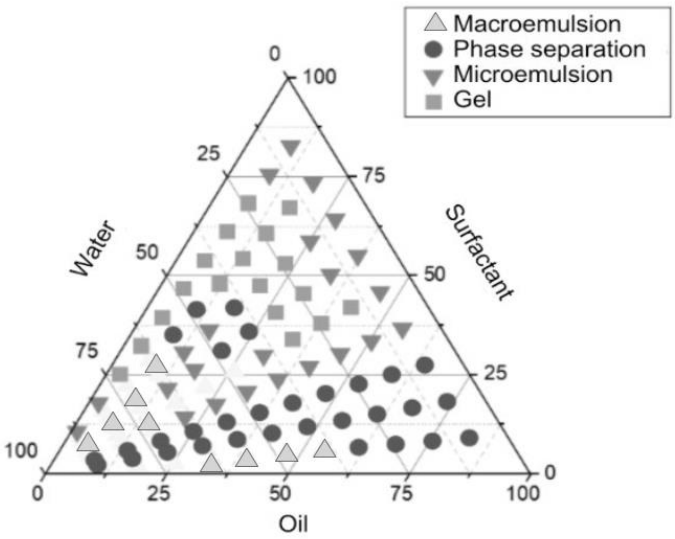

Figure 2: Pseudo-ternary Phase Diagram of BCP Nanoemulsions. Markers represent the different emulsion types formed at varying compositions of oil, surfactant, and water. Formulations were visually classified into macroemulsion (▲), microemulsion (▼), gel (■), and phase separation (●). The diagram illustrates the influence of component ratios on phase behavior and the nanoemulsion formation zone.

Generally, NE are formed in Ternary Phase Diagrams under two main conditions: (i) Low oil and surfactant concentrations with high water content with oil content: up to 10%, surfactant content: up to 20% and water content: above 75%; (ii), moderate to higher oil content with sufficiently high surfactant content: oil content: above 10%, surfactant content: above 10%, water content: variable (typically moderate to high) [40,41]. In these regions, surfactants effectively stabilize small oil droplets dispersed in the continuous aqueous phase, resulting in kinetically stable NE with droplet sizes typically below 200 nm, where the surfactants concentration is sufficient to cover the oil-water interface, preventing coalescence and phase separation [43]. Figure 1 shows that NE was formed when smaller oil (up to 10%) and surfactant amounts (up to 20%) were combined with higher water amounts (above 75%) as well as when higher oil amounts (above 10%) where mixed with higher surfactant amount (above 10%) and variable volumes of water, corroborating previous results from literature with essential oil-based NE and Castor oil-stabilized NE [41,42].

Phase separation occurs when oil concentration is high, but surfactant concentration is low, insufficient to stabilize the oil droplets. This imbalance leads to droplet coalescence and separation of oil and water phases. Indeed, no emulsion was formed at oil-to-surfactant ratios of 8:2 and 9:1 [26,42] which aligns with previous studies. highlighting the critical requirement for sufficient surfactant concentration. Therefore, particle size and PdI were not determined.

Figure 3A and 3B denotes the particle size and PdI of NEs prepared at the following oil/surfactant ratio: 0.5, 0.25, 0.428, 0.66, 1, 1.5 and 2.33. Particle size showed an exponential rise to maximum fitting while for PdI, it was not possible to fit a regression model. The oil: surfactant ratio of 7:3 provided the highest average particle size, i.e., 204±1.03 nm.

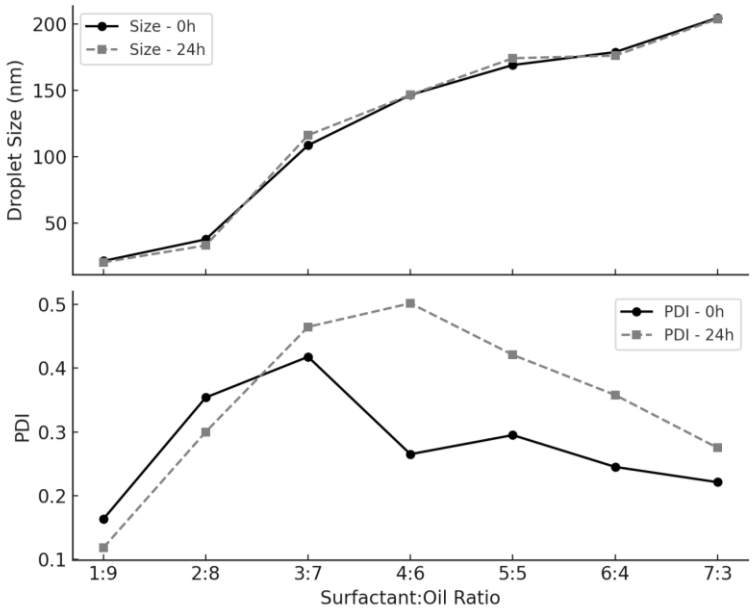

Figure 3: Effect of Surfactant: Oil Ratio on Droplet Size and Polydispersity Index (PdI) at 0 and 24 Hours. Influence of surfactant: oil ratios on average droplet size (3A) and PdI (3B) of BCP-loaded nanoemulsions measured immediately after preparation (0 h) and after 24 hours. At lower oil concentrations (1:9 and 2:8), smaller droplet sizes and lower PdI values were observed, indicating better emulsification and monodispersity.

Studies have shown that the oil/surfactant ratio is a key parameter in controlling NE size distribution, with a linear relationship established between this ratio and particle size [45]. Lower oil/surfactant ratios generally result in smaller particle sizes [46]. The lowest oil: surfactant ratio of 1:9 provided the lowest average particle size, of 21.44 nm ($p<0.05$), confirming an exponential relationship between surfactant dilution and particle size. To oil: surfactant ratio of 5:5 and 6:4 similar particle sizes were obtained ($p>0.05$).

Regarding the polydispersion profile, reflected by PdI values, the oil/ surfactant ratio of 0.11 provided the lowest values (Figure 3B). On the other hand, for oil: surfactant ratio of 3:7, the highest PdI values were found ($p<0.05$). The ratios 1:9 and 2:8 produced monomodal particles after preparation and after 24 hours (Figure 3B). The ratios 3:7, 4:6, 5:5, 6:4, 7:3 showed polydisperse profile, i.e., when more than one particle population after preparation, denoting that these ratios are unsuitable for the development of stable NE. Therefore, the oil/surfactant ratio 1:9 was chosen for further evaluations due to its lower particle size, lower PdI and monomodal particle distribution after preparation.

The hydrophilic-lipophilic balance (HLB) of surfactants affects the phase diagram characteristics and emulsion types formed. The pseudo-ternary phase diagrams provided additional insight into the influence of surfactant and oil concentrations. NE regions were favored at high water content (>75%), moderate surfactant levels (10–20%), and oil concentrations up to 8%, suggesting that optimal droplet formation and stability require not only an appropriate HLB but also a fine-tuned balance of compositional parameters and energy input during emulsification.

The HLB of the surfactant mixture was found to be a critical determinant of both the emulsion type and the phase behavior observed in the pseudo-ternary diagrams constructed during formulation screening. As described by Syed & Peh (2014) [47] ,

specifically, formulations with HLB values between 12 and 14 produced clear, stable NE with low PdI, while values outside this range led to gel formation or phase separation. These results corroborate the idea that proper HLB alignment is essential for minimizing interfacial tension and promoting the formation of thermodynamically favorable droplet curvature.

Although PEG-40 Hydrogenated Castor Oil has a high emulsifying capacity, using it as the sole surfactant can extend the emulsification process. Hence, the combination of more than one surfactant is desirable to reduce interfacial tension, contributing to obtaining a more stable emulsion [37] which once more justify the combination of PEG 40- Hydrogenated Castor Oil and sorbitan monooleate. Sorbitan monooleate and PEG-40 hydrogenated castor oil concentrations were selected based on emulsion E9, as it yielded the smallest particle size with the lowest standard deviation (Figure 1).

To further refine droplet size and promote long-term stability, we adopted a two-step emulsification strategy, combining low-energy aqueous titration with high-energy ultrasonication. A combined approach of low-energy emulsification followed by ultrasonication can produce stable water-in-oil NE with droplet sizes as small as 25 nm [47]. Optimization of process parameters, such as amplitude and sonication time, and analysis of surfactant-to-water ratios are essential for achieving desired nanoemulsion properties and stability [41]. This method was effective for our work as well, since ultrasonication at 90W for 5 minutes in an ice bath consistently yielded droplet sizes smaller than 200 nm, depending on BCP content. The 1:9 oil-to-surfactant ratio emerged as the most effective condition for generating monodisperse droplets, with PdI values below 0.17 even after 90 days of storage.

3.3 Particle Size, PdI, and Colloidal Stability

Nanoemulsions prepared with 6%, 7%, and 8% BCP (designated 6BCP-NE, 7BCP-NE, and 8BCP-NE) and maintaining the 1:9 oil/surfactant ratio was chosen based on its superior colloidal profile. Low oil-to-surfactant ratios (high surfactant content) produce the smallest droplet sizes. For example, an oil: surfactant ratio of 1:9 yielded the smallest particle size in Pseudo ternary diagram experiments (~21 nm), confirming an exponential decrease in droplet size with increasing surfactant dilution. 6BCP-NE (Figure 4), 7BCP-NE (Figure 5), and 8BCP-NE (Figure 6) showed initial particle sizes between 85–100 nm. After preparation, 7BCP-NE and 8BCP-NE had the largest particle size, probably related to their highest oil concentration ($p<0.05$).

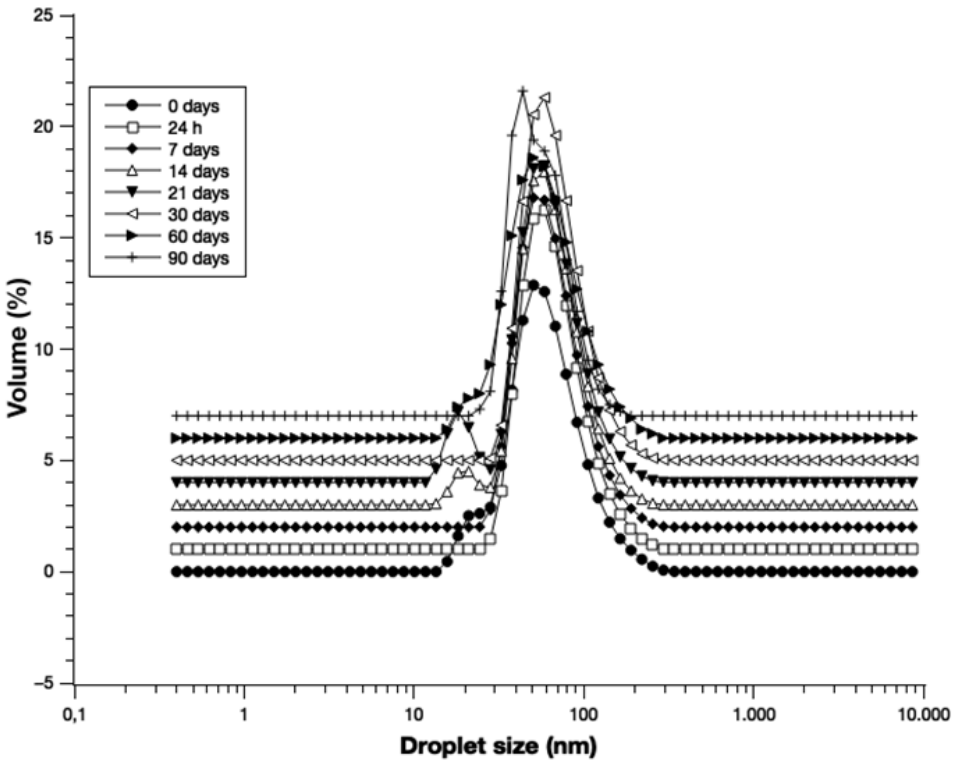

Figure 4: Volume-Based Droplet Size Distribution of 6BCP-NE Over 90 Days of Storage. Temporal evolution of droplet size distribution measured by dynamic light scattering (DLS) from 0 to 90 days.

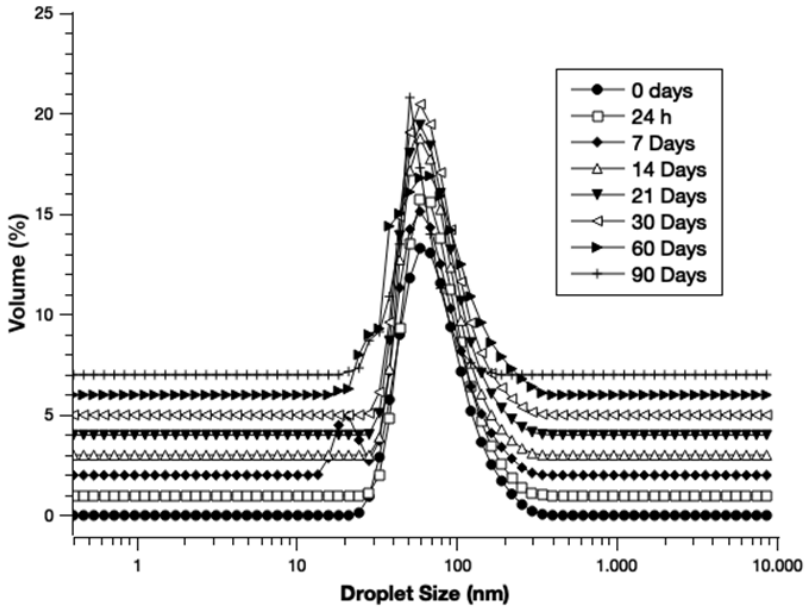

Figure 5: Volume-Based Droplet Size Distribution of 7BCP-NE Over 90 Days of Storage. Temporal evolution of droplet size distribution measured by dynamic light scattering (DLS) from 0 to 90 days.

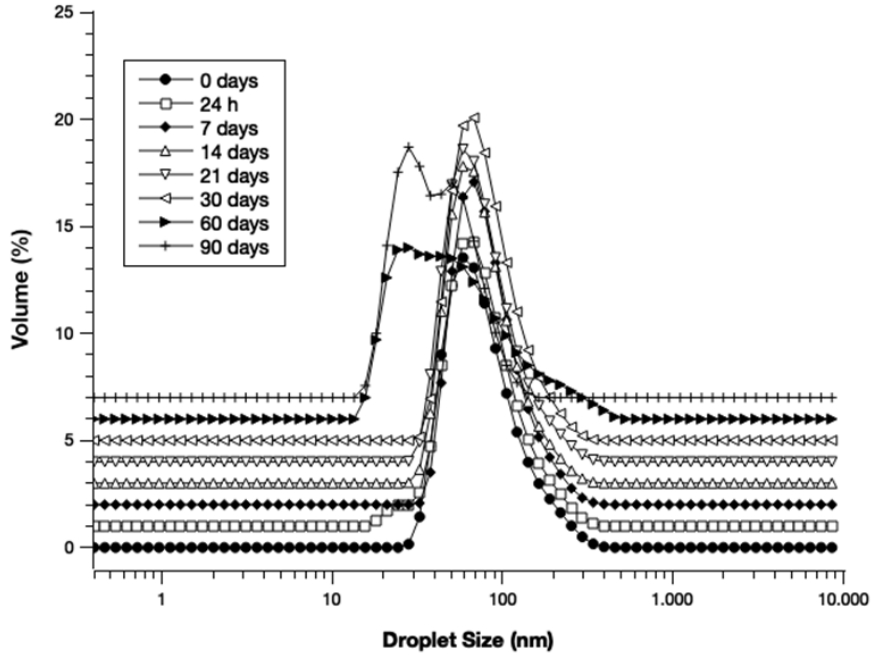

Figure 6: Volume-Based Droplet Size Distribution of 8BCP-NE Over 90 Days of Storage. Temporal evolution of droplet size distribution measured by dynamic light scattering (DLS) from 0 to 90 days.

There were similar particle sizes for 6BCP-NE, 7BCP-NE and 8BCP-NE after 14, 21,28 and 60 days of storage ($p>0.05$) (Figure 7). At the end of storage time, both 7BCP-NE and 8BCP-NE showed an increasing size trend likely due to oil phase coalescence, reaching a higher particle size than 6BCP-NE ($p<0.05$), which maintained the lowest average size until the end of 90 days.

After 90 days of storage, formulations with 7% and 8% BCP showed the largest particle sizes, indicating lower physical stability compared to the 6% BCP-NE ($p<0.05$). This result suggests that higher oil concentrations may accelerate Ostwald ripening, wherein larger droplets grow at the expense of smaller ones due to differential solubility and diffusion effects [48]. Recently [47,48], NE stabilized with PEG-40 hydrogenated castor oil and sorbitan monooleate were prone to Ostwald ripening unless the oil phase was limited and surfactant coverage was sufficient.

The low PdI values (<0.17) are favorable (Figure 7), as lower PdI is often associated with reduced ripening and better shelf stability, reinforcing that 6BCP-NE offers the best kinetic stabilization among the tested formulations. Interestingly, a slight reduction in droplet size was observed between day 14 and day 28 for the 6BCP-NE and 7BCP-NE formulations ($p>0.05$). This phenomenon is likely attributed to surfactant adsorption kinetics at the oil–water interface. After initial homogenization, surfactant molecules may continue to reorganize and equilibrate on the droplet surface, leading to more compact and stabilized interfacial layers, thereby reducing the average particle diameter. This post-equilibration behavior is well-documented in emulsion systems, where delayed surfactant diffusion or rearrangement contributes to increased stabilization and minor size correction over time [49, 50]. By day 60 and day 90, particle sizes of all nanoemulsions converged to values similar to those measured immediately after preparation ($p>0.05$), suggesting that interfacial stabilization was complete.

Notably, 6BCP-NE maintained its initial droplet size without a significant increase throughout storage, indicating exceptional kinetic and thermodynamic stability ($p>0.05$). These findings support the notion that slower equilibration of surfactants, particularly in multi-component systems, can extend stabilization processes beyond the immediate post-preparation phase.

PdI values across all formulations remained consistently below 0.170 during the entire 90-day evaluation period, which is indicative of monodisperse particle size distributions and a high degree of colloidal uniformity. Such low PdI values are crucial for ensuring predictable behavior in nanoformulations, including drug release, shelf-life, and biological interaction. These findings are particularly notable given that prior studies involving β-caryophyllene nanoemulsions have reported higher PdI ranges between 0.200 and 0.300 [51,52] even when using similar surfactant systems.

The improved PdI observed in our study can be attributed to the synergistic stabilization provided by the combination of PEG-40 hydrogenated castor oil and sorbitan monooleate, which likely improved interfacial packing and minimized droplet coalescence during aging. Despite 7BCP-NE and 8BCP-NE exhibiting the largest droplet sizes immediately after preparation and after 90 days, their PdI values remained unchanged, confirming that no new particle populations emerged over time. This indicates that while particle growth may have occurred via mechanisms such as Ostwald ripening, the emulsions maintained monomodal distribution, a hallmark of robust kinetic stability.

In a previous report, BCP nanoemulsions demonstrated stability after 180 days of storage at 4°C and 25°C [54]. Nevertheless, a lower BCP concentration was employed which may explain its higher stability compared to 6BCP-NE, 7BCP-NE, and 8BCP-NE. Hence, the present study highlights the potential for improving the stability

of nanoemulsions composed of BCP, PEG-40 hydrogenated castor oil, and sorbitan monooleate [55].

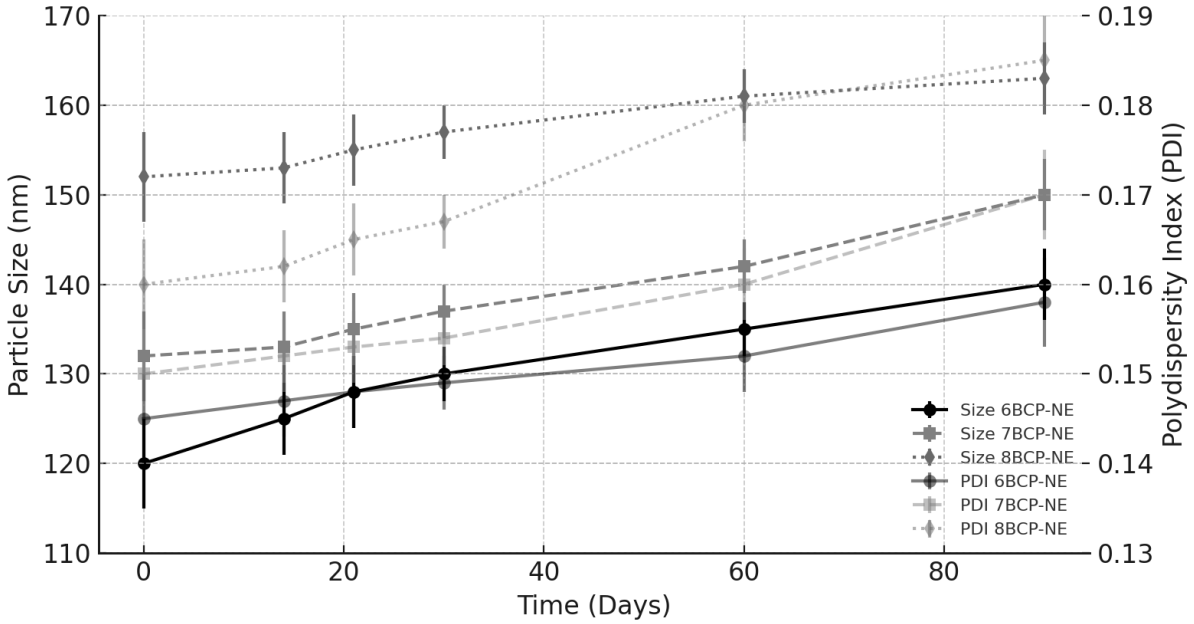

Figure 7: Particle size (A) and PdI values (B) of BCP nanoemulsion over 90 days (mean ±SD). Minimal variation indicates good long-term chemical and interfacial stability**.**

3.4 pH stability

Figure 8 shows a line plot of pH values overage storage. A near-flat line is observed, which indicates stability, while any slight variations can be noticed, increasing the possibility of potential chemical interactions. Overall, pH remained within 6.5 to 6.1 during 90 days, with negligible shifts ($p>0.05$), suitable for topical and oral delivery. The pH values remained nearly constant over the 90-day storage period for all BCP nanoemulsion formulations, with only minor fluctuations (≤0.4 units). This pH stability is a strong indicator of kinetic stability, as it reflects the absence of hydrolytic degradation, emulsifier breakdown, or chemical changes in the dispersed or

continuous phases. In nanoemulsion systems, particularly those containing labile components such as essential oils or terpenes, shifts in pH can signal oxidation, surfactant hydrolysis, or microbial growth [56]. Therefore, the minimal pH variation observed here supports the conclusion that the emulsions remained physicochemical intact under ambient conditions. This finding aligns with other reports where pH stability was used to validate long-term integrity of O/W nanoemulsions containing natural ingredients [57]. It further confirms that the selected surfactant system (PEG-40 hydrogenated castor oil and sorbitan monooleate) not only contributes to interfacial stability but also helps maintain chemical neutrality during storage. The slight deviations might be observed as the nanoemulsion ages (possibly to minor degradation of surfactants or BCP oxidation) but should remain within an acceptable range (e.g., ±0.5 pH units).

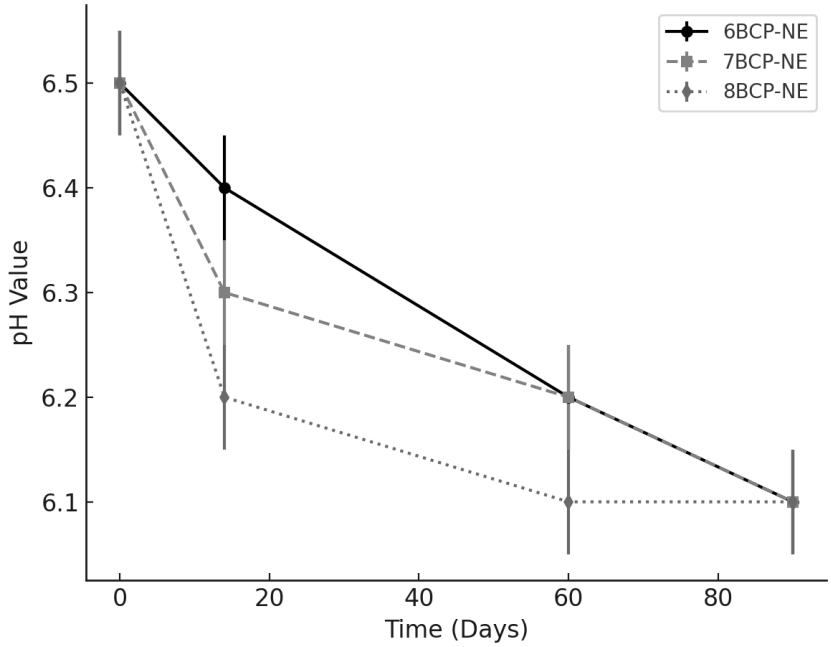

Figure 8: pH values over 90 days of storage for 6BCP-NE, 7BCP-NE and 8CP-NE (mean ± SD). Formulations showed minimal pH variations.

3.5 Thermogravimetric Analysis (TGA)

Isothermal TGA performed at 55 °C (Figure 9) revealed significant differences in the volatilization behavior of neat versus encapsulated BCP. The neat BCP exhibited a rapid, exponential mass loss, retaining only around 20% of its initial content after 4 hours, consistent with its volatile and low-molecular-weight sesquiterpene nature. In contrast, nanoemulsions showed controlled, two-phase kinetics: an initial phase of minimal weight loss (likely due to surface-localized, unencapsulated BCP), followed by a plateau phase, during which BCP loss was gradual and sustained. After 4 hours, more than 70% of BCP remained encapsulated, indicating that nanoemulsification substantially reduces volatility. This phenomenon supports the role of nanoemulsions as diffusion-modulating matrices, wherein the interfacial surfactant shell and aqueous external phase act as a barrier to evaporation.

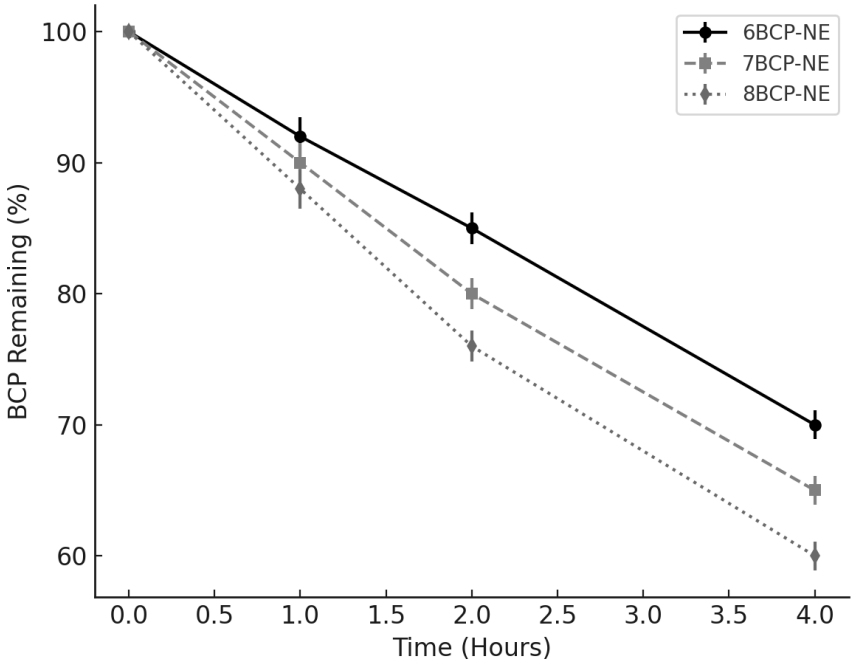

Figure 9: TGA curves showing BCP remaining (%) over time at 55 °C for nanoemulsion (mean ±SD) and neat BCP. Nanoemulsions demonstrated significantly improved volatility control over 4 hours.

As also previously described [10], lipid-based nanoencapsulation significantly retards the release and degradation of phytocannabinoids like BCP by slowing their diffusion from the droplet core. Similarly, encapsulation transforms surface-limited volatilization into a diffusion-governed process, enabling better temporal control of essential oil release and enhancing shelf-life under thermal stress [58]. With these results we clearly show the potential of NE to stabilize thermolabile and volatile compounds, like BCP, making them ideal for pharmaceutical and cosmetic applications where sustained release and ingredient preservation are crucial. With these results we clearly show the potential of NE to stabilize thermolabile and volatile compounds, like BCP, making them ideal for pharmaceutical and cosmetic applications where sustained release and ingredient preservation are crucial.

3.6 Encapsulation Efficiency (EE%) and Drug loading (%)

The calibration curve $y = 60.343x + 0.0812y$ ($R^2 = 0.9953$) was used for both encapsulation efficiency (EE%) and drug loading calculations. Results (Figure 10) show a direct correlation between BCP concentration and drug loading, with values ranging from 5.97% (6BCP-NE) to 7.55% (8BCP-NE).

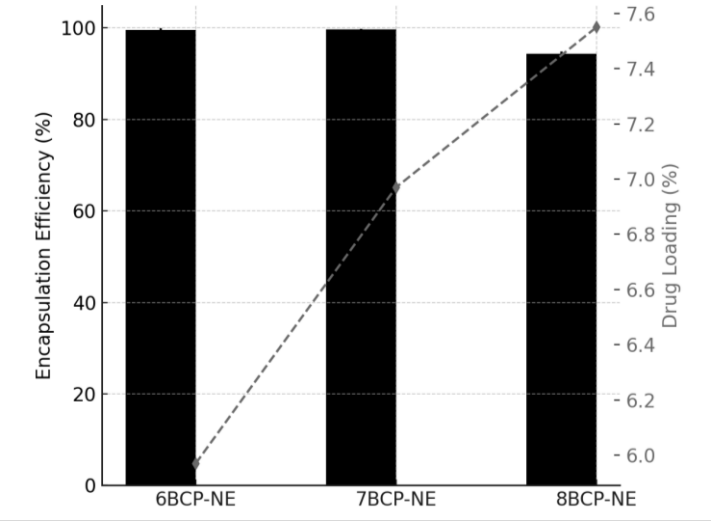

Figure 10: Encapsulation efficiency (EE%) and drug loading of 6BCP-NE, 7BCP-NE and 8BCP-NE. All formulations had an almost complete BCP encapsulation.

All formulations exhibited excellent EE, with 6BCP-NE and 7BCP-NE achieving near-complete encapsulation (>99.5%), while 8BCP-NE retained a still-high 94.36%, albeit with a significant drop compared to lower concentrations ($p < 0.05$)

While EE% values of 6BCP-NE and 7BCP-NE remained exceptionally high (>99%), a statistically significant reduction was observed for 8BCP-NE (94.36% ± 0.45), confirming the saturation effect. Nonetheless, drug loading increased proportionally with BCP concentration, from 5.97% to 7.55%, highlighting a favorable trade-off between loading capacity and encapsulation efficiency. Similar trends have been described for other essential oil-based nanoformulations, wherein an increase in drug concentration boosts the payload but slightly compromises entrapment stability [59]. Despite the minor drop in EE%, the low PdI, high EE%, and substantial drug loading suggest excellent formulation performance. These properties are particularly advantageous in pharmaceutical applications, where reduced dosing volume, improved patient compliance, and enhanced bioavailability are critical design criteria.

3.7 *In vitro* drug release

The in vitro release study of BCP was conducted using a bicompartmental vertical diffusion model with a synthetic membrane, and quantification was performed by HPLC. The results are shown in Figure 11. BCP release was faster and more pronounced in all control samples. This behavior can be explained by the apolar nature of BCF, which exhibits high solubility in ethanol.

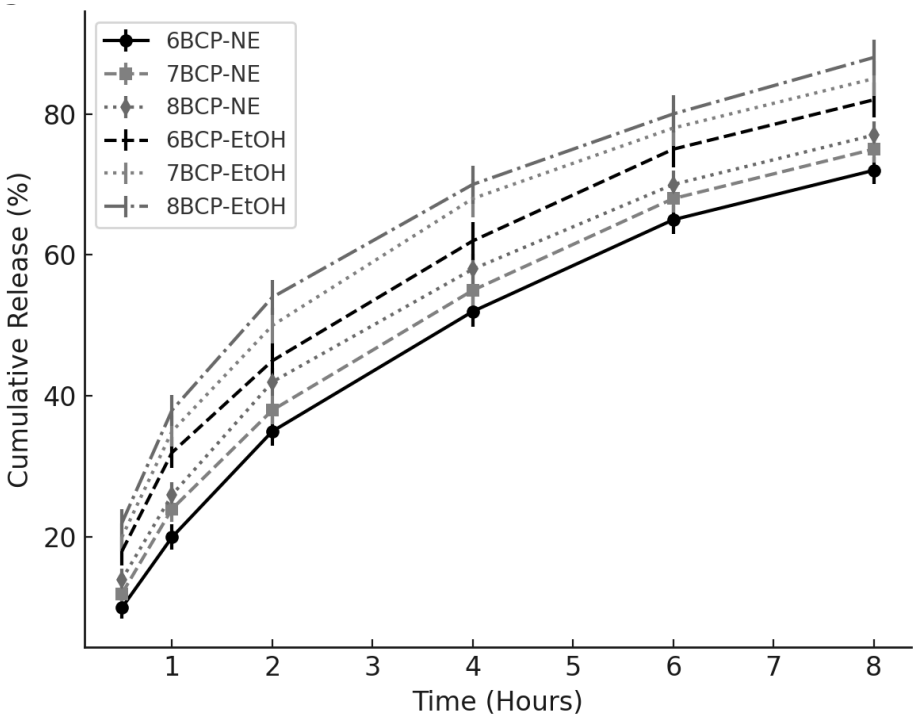

Figure 11: Cumulative in vitro release of BCP from nanoemulsion over 8 hours (mean ±SD). A biphasic release pattern was observed, consistent with initial burst followed by sustained release kinetics.

In vitro release using Franz diffusion cells showed a biphasic release profile featured by an initial burst release (within the first hour) and a sustained release phase, where BCP is steadily diffused out of the nanoemulsion matrix. A rapid release phase occurred within the first hour (12–24%), followed by a sustained release reaching ~75% at 8 hours. The initial burst release is attributed to surface-bound BCP while the

sustained release likely is governed by diffusion through the internal lipid matrix. This release trend aligns with the Higuchi model, which describes drug release as a square-root-of-time-dependent diffusion process from a homogenous matrix system. Such biphasic kinetics are commonly reported in lipid-based nanocarriers and nanoemulsions, where the burst phase ensures rapid therapeutic onset, while the sustained phase provides extended drug availability [60]. The diffusion-controlled release phase is influenced by factors like droplet size, surfactant interfacial thickness, and drug-lipid interactions.

In our study, the fitting of release data to the Higuchi model confirms that diffusion through the nanoemulsion matrix is the predominant release mechanism. This behavior has been previously observed in polymeric and lipid nanoparticles, particularly for lipophilic and poorly water-soluble drugs, where matrix-controlled systems outperform conventional formulations in maintaining prolonged activity [61, 62]. Moreover, the early burst release is likely due to the release of surface-associated BCP, which is in dynamic equilibrium with the external aqueous phase. Once this initial reservoir is depleted, the subsequent release phase becomes governed by diffusion from the encapsulated core, consistent with classical Higuchi-type kinetics.

This controlled profile is a hallmark of NE, in which micellar and nanodroplet architectures act as diffusion barriers, gradually releasing hydrophobic molecules into the external phase. As observed in previous works, the encapsulated BCP molecules maintain equilibrium between internal and external phases, allowing only unbound molecules to diffuse first, followed by matrix-retained BCP that diffuses more slowly [27,63]. These data reinforce the potential of nanoemulsions to provide temporal control over drug bioavailability, enhancing therapeutic windows. Such behavior parallels findings in phytocannabinoid nanoformulations and essential oil-based

delivery systems, where lipid and surfactant components form an effective retention matrix, minimizing burst-related volatility and maximizing controlled release [10, 64].

The release behavior of BCP was clearly influenced by its solubility, its partitioning into micellar and interfacial compartments, and diffusion across the oil–water interface. This mechanism mirrors the physicochemical complexity observed in terpenoid-loaded nanoformulations. In our findings, the initial burst likely arises from BCP near the droplet surface or partially embedded at the surfactant interface, while the prolonged release is attributed to core-retained BCP molecules slowly diffusing through the nanocarrier matrix.

This dual-phase release aligns with previously reported terpenoid nanoemulsion behaviors. In that regard, micelle-interfacial localization plays a pivotal role in regulating terpene diffusion from nanoemulsions [65]. Similarly, the alternating partitioning and interfacial diffusion steps determine release dynamics in oil-in-water systems, particularly for essential oils like limonene or β-caryophyllene [66].

Importantly, the interfacial architecture provided by mixed surfactants (PEG-40 hydrogenated castor oil and sorbitan monooleate) enhances this control by forming rigid boundaries and decreasing interfacial permeability, which are critical to slowing volatile oil escape [67]. These structural features affirm the role of nanoemulsions as advanced diffusion barriers, stabilizing the active compound while ensuring therapeutic availability over time.

Conclusion

This study demonstrates the successful development and optimization of β-caryophyllene (BCP)-loaded nanoemulsions using a systematic approach based on hydrophilic-lipophilic balance (HLB) adjustment, pseudo-ternary phase mapping, and detailed physicochemical characterization. Nanoemulsions with HLB values between 12.9 and 14.3 provided the most stable formulations, with droplet sizes below 160 nm and PdI values < 0.2, indicating monodisperse and kinetically stable systems over 90 days.

The optimized nanoemulsions (6BCP-NE, 7BCP-NE, and 8BCP-NE) achieved encapsulation efficiencies exceeding 94%, with high drug loading and preserved structural integrity. Thermogravimetric analysis confirmed significantly reduced BCP volatility in nanoemulsions compared to neat BCP, reinforcing the barrier effect of nanodroplet encapsulation. In vitro drug release profiles displayed biphasic behavior, characterized by an initial burst followed by sustained release, with a clear delay in release compared to ethanol-based controls. These results highlight the capability of nanoemulsions to modulate and prolong the release of lipophilic volatile compounds.

This report showed that BCP nanoemulsions are a robust and versatile platform for enhancing the stability and controlled delivery of hydrophobic phytochemicals. This formulation approach has broad implications for pharmaceutical and cosmeceutical applications, particularly where volatilization and rapid degradation pose significant formulation challenges.

References

1. Moghrovyan, A.; Parseghyan, L.; Sevoyan, G.; Darbinyan, A.; Sahakyan, N.; Gaboyan, M.; Karabekian, Z.; Voskanyan, A. *Korean J. Pain* **2022**, *35* (2), 140–151. doi:10.3344/kjp.2022.35.2.140.
2. Geddo, F.; Scandiffio, R.; Antoniotti, S.; Cottone, E.; Querio, G.; Maffei, M. E.; Bovolin, P.; Gallo, M. P. *Nutrients* **2019**, *11* (11), 2788. doi:10.3390/nu11112788.
3. Api, A. M.; Belsito, D.; Botelho, D.; Bruze, M.; Burton, G. A.; Buschmann, J.; Dagli, M. L.; Date, M.; Dekant, W.; Deodhar, C.; Francis, M.; Fryer, A. D.; Jones, L.; Joshi, K.; La Cava, S.; Lapczynski, A.; Liebler, D. C.; O'Brien, D.; Patel, A.; Penning, T. M.; Ritacco, G.; Romine, J.; Sadekar, N.; Salvito, D.; Schultz, T. W.; Sipes, I. G.; Sullivan, G.; Thakkar, Y.; Tokura, Y.; Tsang, S. *Food Chem. Toxicol.* **2018**, *122*, S566–S572. doi:10.1016/j.fct.2018.10.020.
4. Ahmed, E. A. *Molecules* **2025**, *30* (8), 1751. doi:10.3390/molecules30081751.
5. Dickson, K.; Scott, C.; White, H.; Zhou, J.; Kelly, M.; Lehmann, C. *Molecules* **2023**, *28* (10). doi:10.3390/molecules28104144.
6. Sharma, C.; M. Al Kaabi, J.; M. Nurulain, S.; N. Goyal, S.; Amjad Kamal, M.; Ojha, S. *Curr. Pharm. Des.* **2016**, *22* (21), 3237–3264. doi:10.2174/1381612822666160311115226.
7. Koyama, S.; Purk, A.; Kaur, M.; Soini, H. A.; Novotny, M. V.; Davis, K.; Kao, C. C.; Matsunami, H.; Mescher, A. *PLoS One* **2019**, *14* (12), e0216104. doi:10.1371/journal.pone.0216104.
8. Viveros-Paredes, J.; González-Castañeda, R.; Gertsch, J.; Chaparro-Huerta, V.; López-Roa, R.; Vázquez-Valls, E.; Beas-Zarate, C.; Camins-Espuny, A.; Flores-Soto, M. *Pharmaceuticals* **2017**, *10* (3), 60. doi:10.3390/ph10030060.
9. Fidyt, K.; Fiedorowicz, A.; Strządała, L.; Szumny, A. *Cancer Med.* **2016**, *5* (10), 3007–3017. doi:10.1002/cam4.816.

10. Santos, P. S.; Oliveira, T. C.; R. Júnior, L. M.; Figueiras, A.; Nunes, L. C. C. *Curr. Pharm. Des.* **2018**, *24* (29), 3440–3453. doi:10.2174/1381612824666180912151412.

11. Santos, P. S.; Souza, L. K. M.; Araújo, T. S. L.; Medeiros, J. V. R.; Nunes, S. C. C.; Carvalho, R. A.; Pais, A. C. C.; Veiga, F. J. B.; Nunes, L. C. C.; Figueiras, A. *ACS Omega* **2017**, *2* (12), 9080–9094. doi:10.1021/acsomega.7b01438.

12. Ghazwani, M.; Hani, U.; Alqarni, M. H.; Alam, A. *Gels* **2023**, *9* (7), 550. doi:10.3390/gels9070550.

13. Alberti, T. B.; Coelho, D. S.; Maraschin, M. *Mater. Sci. Eng. C* **2021**, *121*, 111824. doi:10.1016/j.msec.2020.111824.

14. Dhiman, N.; Awasthi, R.; Sharma, B.; Kharkwal, H.; Kulkarni, G. T. *Front. Chem.* **2021**, *9*. doi:10.3389/fchem.2021.580118.

15. Choi, S. J.; McClements, D. J. *Food Sci. Biotechnol.* **2020**, *29* (2), 149–168. doi:10.1007/s10068-019-00731-4.

16. Barradas, T. N.; de Holanda e Silva, K. G. *Environ. Chem. Lett.* **2021**, *19* (2), 1153–1171. doi:10.1007/s10311-020-01142-2.

17. Hessien, M.; Singh, N.; Kim, C.; Prouzet, E. *Langmuir* **2011**, *27* (6), 2299–2307. doi:10.1021/la104728r.

18. Singpanna, K.; Charnvanich, D. *Thai J. Pharm. Sci.* **2021**, *45* (6), 487–491. doi:10.56808/3027-7922.2530.

19. Hong, I. K.; Kim, S. I.; Lee, S. B. *J. Ind. Eng. Chem.* **2018**, *67*, 123–131. doi:10.1016/j.jiec.2018.06.022.

20. Rodrigues, E. da C. R.; Ferreira, A. M.; Vilhena, J. C. E.; Almeida, F. B.; Cruz, R. A. S.; Florentino, A. C.; Souto, R. N. P.; Carvalho, J. C. T.; Fernandes, C. P. *Rev. Bras. Farmacogn.* **2014**, *24* (6), 699–705. doi:10.1016/j.bjp.2014.10.013.

21. Rodrigues, I. A.; Ramos, A. de S.; Falcão, D. Q.; Ferreira, J. L. P.; Basso, S. L.;

Silva, J. R. de A.; Amaral, A. C. F. *Biomed Res. Int.* **2018**, *2018*, 1–9. doi:10.1155/2018/9781724.

22. Costa, I. C.; Rodrigues, R. F.; Almeida, F. B.; Favacho, H. A.; Falcão, D. Q.; Ferreira, A. M.; Vilhena, J. C. E.; Florentino, A. C.; Carvalho, J. C. T.; Fernandes, C. P. *Lat* **2014**, *33* (January), 459–463.
23. Rodrigues, R. F.; Costa, I. C.; Almeida, F. B.; Cruz, R. A. S.; Ferreira, A. M.; Vilhena, J. C. E.; Florentino, A. C.; Carvalho, J. C. T.; Fernandes, C. P. *Rev. Bras. Farmacogn.* **2015**, *25* (4), 422–425. doi:10.1016/j.bjp.2015.07.014.
24. Fei, T.; Gwinn, K.; Leyva-Gutierrez, F. M. A.; Wang, T. *Heliyon* **2023**, *9* (4), e15101. doi:10.1016/j.heliyon.2023.e15101.
25. Meher, J. G.; Yadav, N. P.; Sahu, J. J.; Sinha, P. *Drug Dev. Ind. Pharm.* **2013**, *39* (10), 1540–1546. doi:10.3109/03639045.2012.719902.
26. Barradas, T. N.; de Campos, V. E. B.; Senna, J. P.; Coutinho, C. dos S. C.; Tebaldi, B. S.; Silva, K. G. de H. e; Mansur, C. R. E. *Colloids Surfaces A Physicochem. Eng. Asp.* **2015**, *480*, 214–221. doi:10.1016/j.colsurfa.2014.12.001.
27. Nogueira, C.; Lemos-Senna, E.; da Silva Vieira, E.; Sampaio, T. B.; Mallmann, M. P.; Oliveira, M. S.; Bernardi, L. S.; Oliveira, P. R. *J. Nanoparticle Res.* **2023**, *25* (1), 19. doi:10.1007/s11051-023-05668-8.
28. Lou, J.; Teng, Z.; Zhang, L.; Yang, J.; Ma, L.; Wang, F.; Tian, X.; An, R.; Yang, M.; Zhang, Q.; Xu, L.; Dong, Z. *Front. Pharmacol.* **2017**, *8*. doi:10.3389/fphar.2017.00002.
29. Alharthi, S.; Ziora, Z. M.; Mustafa, G.; Chaubey, P.; El Kirdasy, A. F.; Alotaibi, G. *Gels* **2023**, *9* (8), 634. doi:10.3390/gels9080634.
30. ICH Harmonised Tripartite Guideline.Validation of Analytical Procedures:text and methodology. Validation of Analytical Procedures:text and methodology.

International Council for Harmonisation 2005.

31. Ekenna, I. C.; Abali, S. O. *J. Drug Deliv. Ther.* **2022**, *12* (2-S), 5–13. doi:10.22270/jddt.v12i2-S.5402.

32. Cheng, K. C.; Khoo, Z. S.; Lo, N. W.; Tan, W. J.; Chemmangattuvalappil, N. G. *Heliyon* **2020**, *6* (5), e03861. doi:10.1016/j.heliyon.2020.e03861.

33. Bunawan, S. N.; Masdor, N. A.; Yasid, N. A.; Halmi, M. I. E.; Shukor, M. Y. A. *Int. J. Nanoelectron. Mater.* **2023**, *16* (Special Issue), 431–440. doi:10.58915/ijneam.v16iDECEMBER.423.

34. Magalhães, B. Q.; Machado, F. P.; Sanches, P. S.; Lima, B.; Falcão, D. Q.; von Ranke, N.; Bello, M. L.; Rodrigues, C. R.; Santos, M. G.; Rocha, L.; Faria, R. X. *Pharmaceutics* **2022**, *14* (5), 911. doi:10.3390/pharmaceutics14050911.

35. Almeida, F.; Corrêa, M.; Zaera, A. M.; Garrigues, T.; Isaac, V. *Colloids Surfaces A Physicochem. Eng. Asp.* **2022**, *643*, 128721. doi:10.1016/j.colsurfa.2022.128721.

36. Saleh, M. N.; Salam, M. A.; Capanoglu, E. *ACS Omega* **2024**. doi:10.1021/acsomega.3c07060.

37. Zeng, L.; Xin, X.; Zhang, Y. *RSC Adv.* **2017**, *7* (32), 19815–19827. doi:10.1039/C6RA27096D.

38. Kunieda, H.; Solans, C.; Shida, N.; Parra, J. L. *Colloids and Surfaces* **1987**, *24* (2–3), 225–237. doi:10.1016/0166-6622(87)80352-9.

39. Liu, Y.; Friberg, S. E. *J. Colloid Interface Sci.* **2009**, *340* (2), 261–268. doi:10.1016/j.jcis.2009.08.038.

40. Kaizu, K.; Alexandridis, P. *J. Colloid Interface Sci.* **2016**, *466*, 138–149. doi:10.1016/j.jcis.2015.10.016.

41. Kumar, H.; Kumar, V. *Ultrason. Sonochem.* **2018**, *49*, 79–88. doi:10.1016/j.ultsonch.2018.07.022.

42. Azeem, A.; Rizwan, M.; Ahmad, F.; Khar, R.; Iqbal, Z.; Talegaonkar, S. *Curr. Nanosci.* **2009**, *5* (2), 220–226. doi:10.2174/157341309788185505.

43. Nirmalayanti, N. L. P. K. V. *Metta J. Ilmu Multidisiplin* **2021**, *1* (3), 158–166. doi:10.37329/metta.v1i3.1552.

44. Ferreira, M. R. A.; Santiago, R. R.; de Souza, T. P.; Egito, E. S. T.; Oliveira, E. E.; Soares, L. A. L. *AAPS PharmSciTech* **2010**, *11* (3), 1383–1390. doi:10.1208/s12249-010-9491-z.

45. Aparicio-Blanco, J.; Sebastián, V.; Rodríguez-Amaro, M.; García-Díaz, H. C.; Torres-Suárez, A. I. *J. Biomed. Nanotechnol.* **2019**, *15* (6), 1149–1161. doi:10.1166/jbn.2019.2765.

46. de Lourdes Pérez-González, M. L.; González-de la Rosa, C. H.; Pérez-Hernández, G.; Beltrán, H. I. *Colloids Surfaces B Biointerfaces* **2020**, *187* (6), 110758. doi:10.1016/j.colsurfb.2019.110758.

47. Syed, H. K.; Peh, K. K. *Acta Pol. Pharm. - Drug Res.* **2014**, *71* (2), 301–309.

48. Mehran, M.; Masoum, S.; Memarzadeh, M. *J. Dispers. Sci. Technol.* **2024**, *46* (1), 108–118. doi:10.1080/01932691.2023.2280093.

49. Rocha-Filho, P. A.; Maruno, M. *Cosmetics* **2025**, *12* (2), 32. doi:10.3390/cosmetics12020032.

50. Delmas, T.; Piraux, H.; Couffin, A.-C.; Texier, I.; Vinet, F.; Poulin, P.; Cates, M. E.; Bibette, J. *Langmuir* **2011**, *27* (5), 1683–1692. doi:10.1021/la104221q.

51. Nejadmansouri, M.; Hosseini, S. M. H.; Niakosari, M.; Yousefi, G. H.; Golmakani, M. T. *Colloids Surfaces A Physicochem. Eng. Asp.* **2016**, *506*, 821–832. doi:10.1016/j.colsurfa.2016.07.075.

52. Weimer, P.; de Araújo Lock, G.; Amaral Antunes Nunes, K.; Rossi, R. C.; Koester, L. S. *Nat. Prod. Res.* **2024**, 1–7. doi:10.1080/14786419.2024.2317887.

53. Pinto, E. P.; Menezes, R. P.; Pires, M. A.; Zamora, R. R. M.; Araújo, R. S.;

Souza, T. M. de. *Mater. Today Commun.* **2023**, *35*, 105765. doi:10.1016/j.mtcomm.2023.105765.

54. Santos Porto, D.; da Costa Bernardo Port, B.; Conte, J.; Fretes Argenta, D.; Pereira Balleste, M.; Amadeu Micke, G.; Machado Campos, Â.; Silva Caumo, K.; Caon, T. *Int. J. Pharm.* **2024**, *659* (May). doi:10.1016/j.ijpharm.2024.124252.
55. Pavoni, L.; Perinelli, D. R.; Ciacciarelli, A.; Quassinti, L.; Bramucci, M.; Miano, A.; Casettari, L.; Cespi, M.; Bonacucina, G.; Palmieri, G. F. *J. Drug Deliv. Sci. Technol.* **2020**, *58*, 101772. doi:10.1016/j.jddst.2020.101772.
56. O'Neill, M. A. A.; Gaisford, S. *Int. J. Pharm.* **2011**, *417* (1–2), 83–93. doi:10.1016/j.ijpharm.2011.01.038.
57. Laskowska, M.; Pastukh, O.; Konieczny, P.; Dulski, M.; Zalsiński, M.; Laskowski, L. *Materials (Basel).* **2020**, *13* (11), 2624. doi:10.3390/ma13112624.
58. Lu, L.; Yu, R.; Zhang, L. *Food Chem.* **2023**, *421*, 136205. doi:10.1016/j.foodchem.2023.136254.
59. Montenegro, L.; Pasquinucci, L.; Zappalà, A.; Chiechio, S.; Turnaturi, R.; Parenti, C. *Pharmaceutics* **2017**, *9* (4), 48. doi:10.3390/pharmaceutics9040048.
60. Dandamudi, M.; McLoughlin, P.; Behl, G.; Rani, S.; Coffey, L.; Chauhan, A.; Kent, D.; Fitzhenry, L. *Pharmaceutics* **2021**, *13* (10), 1590. doi:10.3390/pharmaceutics13101590.
61. Soltani, S.; Zakeri-Milani, P.; Barzegar-Jalali, M.; Jelvehgari, M. *Iran. J. Basic Med. Sci.* **2016**, *19* (5), 850–860.
62. Castillo-Henríquez, L.; Vargas-Zúñiga, R.; Pacheco-Molina, J.; Vega-Baudrit, J. *ADMET DMPK* **2020**. doi:10.5599/admet.844.
63. Zhou, K.; Liu, Z.; Fan, R.; Zhao, M.; Luo, L.; Wang, Y.; Jiang, Y.; Lu, Z.; Tang, J.; Luo, A.; Guan, T.; Sun, H.; Zhou, T.; Dai, C. *Int. J. Pharm.* **2023**, *638*, 122923. doi:10.1016/j.ijpharm.2023.122923.

64. Zhu, T.; Gao, W.; Fang, D.; Liu, Z.; Wu, G.; Zhou, M.; Wan, M.; Mao, C. *Mater. Sci. Eng. C* **2021**, *120*, 111725. doi:10.1016/j.msec.2020.111725.

65. Miastkowska, M.; Śliwa, P. *Molecules* **2020**, *25* (12), 2747. doi:10.3390/molecules25122747.

66. Shaker, D. S.; Ishak, R. A. H.; Ghoneim, A.; Elhuoni, M. A. *Sci. Pharm.* **2019**, *87* (3), 17. doi:10.3390/scipharm87030017.

67. Barradas, T. N.; de Holanda e Silva, K. G. Nanoemulsions as Optimized Vehicles for Essential Oils. In *Sustainable Agriculture Reviews 44*; Saneja, A., Panda, A., Lichtfouse, E., Ed.; Springer: Cham, 2020; pp 115–167. doi:10.1007/978-3-030-41842-7_4.